JOURNAL OF GUIDANCE, CONTROL, AND DYNAMICS
Vol. 41, No. 5, May 2018



# Engineering Notes

## Optimal Rendezvous Guidance Laws with Application to Civil Autonomous Aerial Refueling

A. Tsukerman,* M. Weiss,† and T. Shima‡
*Technion–Israel Institute of Technology, 32000 Haifa, Israel*
and
D. Löbl§ and F. Holzapfel¶
*Technical University of Munich, 85748 Munich, Germany*

DOI: 10.2514/1.G003154



### I. Introduction

AERIAL refueling is the process of transferring fuel from one aircraft (the tanker) to another (the receiver) during flight. It has been used as a standard method to increase range and endurance of military aircraft. In the last couple of years, research has been conducted in the framework of a European project, called RECREATE (from "Research on a Cruiser Enabled Air Transport Environment") [1], where aerial refueling has been proposed as a new paradigm to help reduce the environmental impact and improve the fuel efficiency of long-haul air transportation. According to this paradigm, the flight mission can be split into sections, to allow a passenger aircraft to take off with much less fuel onboard than required to fly the whole mission. Dedicated aircraft (the tanker) can rendezvous with the passenger aircraft (the receiver) along its route and transfer the required amount of fuel to fly the whole mission. The basic idea is that, if weight is reduced due to smaller amount of fuel at takeoff, the whole aircraft structure can be lighter, and for a given range, the overall fuel consumption (of both the passenger aircraft and the tanker) can be reduced [2]. The performance tradeoff, which was carried out in the framework of RECREATE, indicated the operational need to exploit the boom-and-receptacle aerial refueling system [3] and ensure passengers' comfort by avoiding significant receiver maneuvers, which may induce accelerations and noise. Therefore, it is desired to operate mainly the tanker to complete the mission while the receiver maintains the original flight route. Furthermore, aerial refueling, as a manually piloted procedure today, has proven to be an extremely difficult and demanding task for pilots. Therefore, automation becomes a necessity to reduce the workload of the tanker pilots (as mentioned previously, in this scenario, the tanker performs the required maneuver and not the receiver). Alternatively, fully autonomous aerial refueling will allow some cost savings. The execution of an automatic approach maneuver is naturally related to the guidance and control field; therefore, methods and techniques from this field of study can be applied for solving and analyzing this problem.

Attempts to employ classical guidance laws, mainly used for missile intercept applications, such as proportional navigation (PN) and pure pursuit for the purpose of autonomous aerial refueling and formation flight were made over the past years [4,5]. Modern guidance and control techniques were employed to solve autonomous aerial refueling in the past. In [6], an adaptive neural-network-based autopilot for automatic approach was presented. The autopilot was tested in a six-degree-of-freedom (6-DOF) simulation model exhibiting guaranteed performance specifications. In [7,8], the authors developed and demonstrated machine-vision-based algorithms integrated with guidance and control algorithms for both autonomous boom-and-receptacle and probe-and-drogue aerial refueling systems to achieve smooth approach and docking. In [9], an approach reference trajectory was designed and tracked. The errors were estimated using a state observer and regulated using a controller designed based on linear quadratic regulator theory.

Inspired by missile interception guidance methods with intercept angle constraints [10–12], this paper presents two novel optimal rendezvous guidance laws. The guidance problem is formulated as a terminal intercept problem explicitly constraining terminal position, terminal flight-path angle, and terminal acceleration. This formulation is used to shape the trajectory of the tanker such that its velocity vector will align with the velocity vector of the receiver near the rendezvous point, avoiding further maneuvering. Two guidance laws are derived. The first is designed as outer loop based on a first-order lag model of an inner autopilot loop. The second is derived as a single-loop autopilot-guidance controller, which is based on a more detailed airframe model, using full state feedback. The guidance and control schemes are implemented in a detailed, nonlinear, 6-DOF simulation model, and the performance of the proposed guidance laws is investigated and compared based on simulation results.

The rest of the paper is structured as follows. In Sec. II, the mathematical models and formulations, used throughout the paper, are presented. In Sec. III, the linear–quadratic optimal guidance problem is posed, and the solution is given and analyzed. The performance evaluation is performed in Sec. IV. Finally, conclusions are drawn in Sec. V.

### II. Mathematical Models

Consider the aerial refueling approach scenario in Fig. 1. The approach is initiated when the receiver and tanker are flying roughly on the same path; the receiver is assumed to fly straight and level. The positions of the tanker and receiver center of gravity in a Cartesian inertial reference frame $X_E$–$Y_E$–$Z_E$ (local level north–east–down) are denoted as $\boldsymbol{r}_T$ and $\boldsymbol{r}_R$, respectively. The tanker speed, climb angle, course angle, and acceleration are denoted as $V_T$, $\gamma_T$, $\chi_T$, and $\boldsymbol{a}_T$, respectively. The receiver speed, climb angle, course angle, and acceleration are denoted as $V_R$, $\gamma_R$, $\chi_R$, and $\boldsymbol{a}_R$, respectively. The relative displacement between tanker and receiver is written as

$$\boldsymbol{r} = \boldsymbol{r}_T - \boldsymbol{r}_R = [x \quad y \quad z] \tag{1}$$

The inertial acceleration of the tanker and the receiver is written in terms of its components as $\boldsymbol{a}_T = [a_{T_x} \quad a_{T_y} \quad a_{T_z}]$ and $\boldsymbol{a}_R = [a_{R_x} \quad a_{R_y} \quad a_{R_z}]$, respectively. The equations of motion associated with the relative position errors and flight-path angular errors (assuming $\gamma_R = \chi_R = 0$) are

Presented at the 2017 AIAA SciTech, Grapevine, TX, 9–13 June 2017; received 26 June 2017; revision received 13 November 2017; accepted for publication 21 January 2018; published online 30 March 2018. 

*M.Sc. Student, Technion Autonomous Systems Program.
†Research Staff, Faculty of Aerospace Engineering.
‡Professor, Faculty of Aerospace Engineering.
§Research Associate, Institute of Flight System Dynamics.
¶Full Professor, Head of Institute, Institute of Flight System Dyamics.

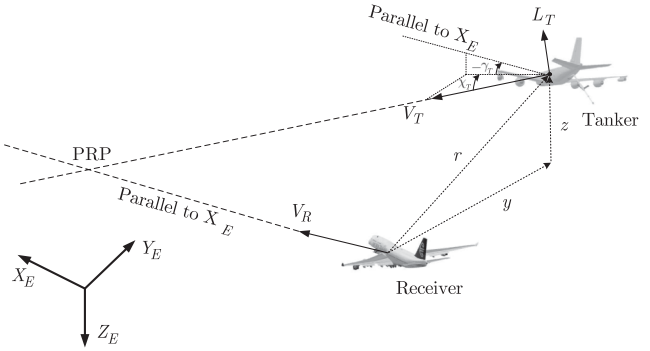


**Fig. 1 Relative geometry of the approach maneuver.**

$$\begin{cases} \dot{x} = V_T \cos\chi_T \cos\gamma_T - V_R \cos\chi_R \cos\gamma_R \\ \dot{y} = V_T \sin\chi_T \cos\gamma_T - V_R \sin\chi_R \cos\gamma_R \\ \dot{z} = V_T \sin\gamma_T - V_R \sin\gamma_R \\ \dot{\gamma}_T = L_T \cos\phi_T / m_T V_T + g \cos\gamma_T / V_T \\ \dot{\chi}_T = L_T \sin\phi_T / m_T V_T \cos\gamma_T \end{cases} \tag{2}$$

where $m_T$, $L_T$, and $\phi_T$ are the tanker's mass, lift, and roll angle, respectively. The following assumptions are used. Because of small deviations from trim state, the flight dynamics of the tanker relative to the receiver can be separated into two perpendicular channels [13]. Also, it is assumed that the tanker's speed $V_T$ is controlled separately using thrust commands for regulating $a_{T_x}$ to achieve position and velocity matching of the tanker with respect to the receiver in the $x$ coordinate. The explicit computation of the required thrust commands is not addressed in this work. Furthermore, as expected for aerial refueling, the variation in speed is small, and $V_T$ will be assumed constant for the derivation of the guidance laws. Therefore, the equation corresponding to $\dot{x}$ is removed. The preceding assumptions are used to linearize and reduce the relative kinematics model in Eq. (2) to a simpler form as

$$\begin{cases} \dot{y} = V_T \chi_T \\ \dot{z} = V_T \gamma_T \\ \dot{\gamma}_T = a_{T_z} / V_T \\ \dot{\chi}_T = a_{T_y} / V_T \end{cases} \tag{3}$$

where

$$a_{T_z} \triangleq L_T / m_T + g, \qquad a_{T_y} \triangleq L_T \phi_T / m_T \tag{4}$$

### A. Separated Guidance and Autopilot

In the separated guidance law and control (SGC), an existing autopilot is used, and a separated guidance law is developed based on a simple kinematic model. To enhance the guidance system performance, the autopilot response can be explicitly taken into account in the guidance law design. In this work, first-order differential equations are used to model the autopilot and airframe response to acceleration commands:

$$\dot{a}_{T_y} = -\frac{1}{\tau_{T_y}} a_{T_y} + \frac{1}{\tau_{T_y}} a^c_{T_y}, \quad \dot{a}_{T_z} = -\frac{1}{\tau_{T_z}} a_{T_z} + \frac{1}{\tau_{T_z}} a^c_{T_z} \tag{5}$$

where $a^c_{T_y}$ and $a^c_{T_z}$ are the acceleration commands issued to the lateral and longitudinal autopilot, respectively. $\tau_{T_y}$ and $\tau_{T_z}$ are the corresponding time constants. The model that will be used in the next section for SGC derivation is now presented for the vertical channel. The state vector is composed of the vertical position error and relative flight-path angle, and it is augmented with Eq. (5):

$$\boldsymbol{x} = [\, z \quad \gamma_T \quad a_{T_z} \,]^T, \qquad u_{T_z} = a^c_{T_z} \tag{6}$$

and the equations of motion associated with $\boldsymbol{x}$ are

$$\dot{\boldsymbol{x}} = \begin{cases} \dot{x}_1 = V_T x_2 \\ \dot{x}_2 = x_3 / V_T \\ \dot{x}_3 = -\dfrac{1}{\tau_{T_z}} x_3 + \dfrac{1}{\tau_{T_z}} u_{T_z} \end{cases} \tag{7}$$

Equation (7) is written in matrix form as

$$\dot{\boldsymbol{x}} = \boldsymbol{A}\boldsymbol{x} + \boldsymbol{B} u_{T_z} \tag{8}$$

where

$$\boldsymbol{A} = \begin{bmatrix} 0 & V_T & 0 \\ 0 & 0 & 1/V_T \\ 0 & 0 & -\dfrac{1}{\tau_{T_z}} \end{bmatrix} \qquad \boldsymbol{B} = \begin{bmatrix} 0 \\ 0 \\ \dfrac{1}{\tau_{T_z}} \end{bmatrix}$$

The same design model is used for the horizontal channel with

$$\boldsymbol{x} = [\, y \quad \chi_T \quad a_{T_y} \,]^T \tag{9}$$

and the corresponding autopilot lag $\tau_{T_y}$.

### B. Integrated Guidance–Autopilot

Integrated guidance–autopilot (IGC) design is based on a more complex model of the system, and it delivers a combined guidance and control algorithm [14]. Here, the longitudinal and lateral linear dynamic models of the tanker airframe are used. The models are structured using the dimensional stability and control derivatives of the aircraft. These derivatives result from linearization of the equations of motion of the aircraft and describe the change in the forces and moments acting on the aircraft due to small perturbations from the trim conditions. The dimensional stability and control derivatives are used to model the rate of change of angle of attack $\alpha$, pitch angle $\theta$, and pitch rate $q$. The elevator servo response $\delta_e$ is approximated as a first-order lag with time constant $\tau_e$. The longitudinal dynamics are written as a system of differential equations:

$$\begin{cases} \dot{\alpha} = Z_\alpha \alpha + Z_q q + Z_{\delta_e} \delta_e \\ \dot{\theta} = q \\ \dot{q} = M_\alpha \alpha + M_q q + M_{\delta_e} \delta_e \\ \dot{\delta}_e = -\dfrac{1}{\tau_e} \delta_e + \dfrac{1}{\tau_e} \delta^c_e \end{cases} \tag{10}$$

The longitudinal state vector is selected as

$$\boldsymbol{x}_{T_z} = [\, \alpha \quad \theta \quad q \quad \delta_e \,]^T \tag{11}$$

System (10) is written in state-space form as

$$\dot{\boldsymbol{x}}_{T_z} = \boldsymbol{A}_{T_z} \boldsymbol{x}_{T_z} + \boldsymbol{B}_{T_z} u_{T_z} \tag{12}$$

where

$$\boldsymbol{A}_{T_z} = \begin{bmatrix} Z_\alpha & 0 & Z_q & Z_{\delta_e} \\ 0 & 0 & 1 & 0 \\ M_\alpha & 0 & M_q & M_{\delta_e} \\ 0 & 0 & 0 & -1/\tau_e \end{bmatrix}$$

$$\boldsymbol{B}_{T_z} = [\, 0 \quad 0 \quad 1/\tau_e \,]^T \tag{13}$$

The maneuvering acceleration can be modeled as a function of the path angular rate that can be expressed in terms of the state-space vector using

$$a_{T_z} = V_T\dot{\gamma}_T = V_T(q - \dot{\alpha}) \tag{14}$$

Consequently, $a_{T_z}$ can be written as

$$a_{T_z} = \boldsymbol{C}_{T_z}\boldsymbol{x}_{T_z} \tag{15}$$

where

$$\boldsymbol{C}_{T_z} = V_T\begin{bmatrix} -Z_\alpha & 0 & (1 - Z_q) & -Z_{\delta_e} \end{bmatrix} \tag{16}$$

For IGC design, the augmented model [Eq. (8)] is formed with

$$\boldsymbol{x} = [\, z \quad \gamma_T \quad \boldsymbol{x}_{T_z}\,]^T, \qquad u_{T_z} = \delta_e^c \tag{17}$$

where the corresponding model matrices are

$$\boldsymbol{A}_z = \begin{bmatrix} \boldsymbol{A}_1 & \boldsymbol{A}_{12} \\ 0_{4\times 2} & \boldsymbol{A}_{T_z} \end{bmatrix}, \qquad \boldsymbol{B}_z = \begin{bmatrix} 0 \\ 0 \\ \boldsymbol{B}_{T_z} \end{bmatrix}$$

$$\boldsymbol{A}_1 = \begin{bmatrix} 0 & V_T \\ 0 & 0 \end{bmatrix}, \qquad \boldsymbol{A}_{12} = \begin{bmatrix} 0_{1\times 4} \\ \dfrac{1}{V_T}\boldsymbol{C}_{T_z} \end{bmatrix}$$

The lateral motion model is structured similar to the longitudinal model. Here, $\beta$ is the angle of sideslip, $r$ is the yaw rate, $\phi$ is the roll angle, and $p$ is the roll rate. The aileron servo response $\delta_a$ is modeled as a first-order lag with time constant $\tau_a$. The linear equations of motion, written as a system of differential equations using the lateral-directional dimensional stability derivatives are

$$\begin{cases} \dot{\beta} = Y_v\beta + Y_r r + g\phi/V_T + Y_p p + Y_{\delta_a}\delta_a/V_T \\ \dot{r} = N_\beta\beta + N_r r + N_p p + N_{\delta_a}\delta_a \\ \dot{\phi} = p \\ \dot{p} = L_\beta\beta + L_r r + L_p p + L_{\delta_a}\delta_a \\ \dot{\delta}_a = -\dfrac{1}{\tau_a}\delta_a + \dfrac{1}{\tau_a}\delta_a^c \end{cases} \tag{18}$$

The dynamic model is formulated using the following state vector:

$$\boldsymbol{x}_{T_y} = [\beta \quad r \quad \phi \quad p \quad \delta_a\,]^T \tag{19}$$

and the corresponding state-space representation is

$$\dot{\boldsymbol{x}}_{T_y} = \boldsymbol{A}_{T_y}\boldsymbol{x}_{T_y} + \boldsymbol{B}_{T_y}u_{T_y}$$

where

$$\boldsymbol{A}_{T_y} = \begin{bmatrix} Y_v & Y_r & g/V_T & Y_p & Y_{\delta_a}/V_T \\ N_\beta & N_r & 0 & N_p & N_{\delta_a} \\ 0 & 0 & 0 & 1 & 0 \\ L_\beta & L_r & 0 & L_p & L_{\delta_a} \\ 0 & 0 & 0 & 0 & -1/\tau_a \end{bmatrix}$$

$$\boldsymbol{B}_{T_y} = [0 \quad 0 \quad 0 \quad 1/\tau_a\,]^T$$

The maneuvering acceleration in the lateral plane of motion is modeled as

$$a_{T_y} = V_T\dot{\chi}_T = V_T(r - \dot{\beta}) \tag{20}$$

Therefore, $a_{T_y}$ can be written as

$$a_{T_y} = \boldsymbol{C}_{T_y}\boldsymbol{x}_{T_y} \tag{21}$$

where

$$\boldsymbol{C}_{T_y} = V_T\begin{bmatrix} -Y_v & (1 - Y_r) & -g/V_T & -Y_p & -Y_{\delta_a}/V_T \end{bmatrix} \tag{22}$$

Now, the augmented model [Eq. (8)] is formed with

$$\boldsymbol{x} = \begin{bmatrix} y & \chi_T & \boldsymbol{x}_{T_y} \end{bmatrix}^T, \qquad u_{T_y} = \delta_a^c \tag{23}$$

where the corresponding model matrices are

$$\boldsymbol{A}_y = \begin{bmatrix} \boldsymbol{A}_1 & \boldsymbol{A}_{12} \\ 0_{5\times 2} & \boldsymbol{A}_{T_y} \end{bmatrix}, \qquad \boldsymbol{B}_y = \begin{bmatrix} 0 \\ 0 \\ \boldsymbol{B}_{T_y} \end{bmatrix}$$

$$\boldsymbol{A}_1 = \begin{bmatrix} 0 & V_T \\ 0 & 0 \end{bmatrix}, \qquad \boldsymbol{A}_{12} = \begin{bmatrix} 0_{1\times 5} \\ \dfrac{1}{V_T}\boldsymbol{C}_{T_y} \end{bmatrix}$$

## III. Guidance Law Derivation

In this section, we pose and solve the linear quadratic optimal control problem. The cost function is selected such that rendezvous will occur at $t_f$. $t_f$ is dependent on the assumed thrust controller which is responsible for achieving speed matching, namely $V_T = V_R$. It is assumed that $t_f$ can be estimated continuously during the entire maneuver. Position matching is imposed by minimizing position errors $(z, y)$ relative to the desired docking formation. Horizontal and vertical velocity matching is achieved by minimizing the relative flight-path angular errors $(\gamma_I, \chi_I)$. Additionally, the cost is supplemented with an acceleration term $(a_{T_x}, a_{T_y})$ because, unlike in a missile interception problem, it is important to maintain the aircraft alignment and reduce maneuvering at the end of the approach phase. The standard general formalism for the linear quadratic cost function is used:

$$J = \boldsymbol{x}(t_f)^T\boldsymbol{Q}_f\boldsymbol{x}(t_f) + \int_{t_0}^{t_f}\left\{\boldsymbol{x}(t)^T\boldsymbol{Q}(t)\boldsymbol{x}(t) + u^T\boldsymbol{R}u\right\}\mathrm{d}t \tag{24}$$

where $\boldsymbol{x}$ and $u$ are selected according to the required design model [Eqs. (8), (17), and (23)], and the appropriate weight matrices are

$$\boldsymbol{Q}_f = \begin{bmatrix} \boldsymbol{Q}_{f_{11}} & 0_{2\times n} \\ 0_{n\times 2} & \boldsymbol{Q}_{f_{22}} \end{bmatrix}, \qquad \boldsymbol{R} = \mu, \qquad \boldsymbol{Q} = 0_{(n+2)\times(n+2)}$$

$$\boldsymbol{Q}_{f_{11}} = \begin{bmatrix} c_1 & 0 \\ 0 & c_2 \end{bmatrix}, \qquad \boldsymbol{Q}_{f_{22}} = c_3\boldsymbol{C}_T^T\boldsymbol{C}_T$$

where $n$ is the order of the airframe dynamic model. The guidance law is then obtained as a full state feedback controller

$$u = -\boldsymbol{R}^{-1}\boldsymbol{B}^T\boldsymbol{P}(t_{\mathrm{go}})\boldsymbol{x}(t) = \boldsymbol{N}(t_{\mathrm{go}})\boldsymbol{x}(t) \tag{25}$$

### A. Analysis of the Separated Guidance Law

In this section, the closed-form solution for the separated guidance law is presented, and limiting cases are developed and compared to previous results. For these purposes, the SGC full-state feedback will be written in terms of the vector $\boldsymbol{Z}$, and the autopilot lag will be represented using $\tau_T$. This vector is defined using the so-called terminal projection transformation [10] corresponding to Eq. (7) as

$$\boldsymbol{Z} = \boldsymbol{D}\Phi_A(t_f, t)\boldsymbol{x}(t) \tag{26}$$

where

$$\boldsymbol{D} = \begin{bmatrix} 1 & 0 & 0 \\ 0 & 1 & 0 \\ 0 & 0 & 1 \end{bmatrix}, \qquad \Phi_A(t_f, t) = e^{At_{\text{go}}}$$

The new state vector $\boldsymbol{Z}$ has an important physical meaning. $Z_1(t)$ is known as the zero-effort miss (ZEM) [15], which, in our one-sided optimization problem, is the miss distance if, from the current time onward, the tanker will not apply any control and the receiver will not maneuver. $Z_2(t)$ is the zero-effort speed (ZES), which, in an analogy to the ZEM, is the relative speed error if, from the current time onward, the tanker will not apply any control and the receiver will not maneuver. $Z_3(t)$ is the zero-effort acceleration (ZEA), which is the tanker's acceleration if, from the current time onward, the tanker will not apply any control and the receiver will not maneuver:

$$\boldsymbol{Z} = \begin{cases} \text{ZEM} = x_1 + V_T t_{\text{go}} x_2 + \tau_T^2 \psi_1(\sigma) x_3 \\ \text{ZES} = V_T x_2 - \tau_T \psi_2(\sigma) x_3 \\ \text{ZEA} = \psi_3(\sigma) x_3 \end{cases} \tag{27}$$

where

$$\psi_1(\sigma) \triangleq \sigma + e^{-\sigma} - 1, \quad \psi_2(\sigma) \triangleq e^{-\sigma} - 1, \quad \psi_3(\sigma) \triangleq e^{-\sigma}, \quad \sigma = t_{\text{go}}/\tau_T \tag{28}$$

The guidance law in Eq. (25) can now be written in terms of the zero effort vector as

$$u = \frac{N_1(t_{\text{go}})}{t_{\text{go}}^2}\text{ZEM}(t_{\text{go}}) + \frac{N_2(t_{\text{go}})}{t_{\text{go}}}\text{ZES}(t_{\text{go}}) + N_3(t_{\text{go}})\text{ZEA}(t_{\text{go}}) \tag{29}$$

The gains are obtained in closed form as functions of the time-varying integrals given next for a few interesting particular cases. For perfect intercept and for perfect intercept angle only, we need to select $c_1, c_2 \to \infty$, and $c_3 \to 0$:

$$N_1(c_1, c_2 \to \infty, c_3 \to 0) = \frac{V_T^2(\psi_1 I_2 - \psi_2 I_{12})}{\tau_T D(\sigma)} \tag{30}$$

$$N_2(c_1, c_2 \to \infty, c_3 \to 0) = \frac{V_T(\psi_1 I_2 - \psi_2 I_{12})}{\tau_T^2 D(\sigma)} \tag{31}$$

$$N_3(\sigma) = 0 \tag{32}$$

where

$$D(\sigma) \triangleq \frac{V_T^2}{\tau_T^4}(I_{12}^2 - I_1 I_2)$$

$$I_1 \triangleq \int_t^{t_f} \tau_T^4 \psi_1(\sigma)^2 \, \mathrm{d}\sigma, \qquad I_{13} \triangleq \int_t^{t_f} \tau_T^2 \psi_1(\sigma)\psi_3(\sigma) \, \mathrm{d}\sigma$$

$$I_{12} \triangleq \int_t^{t_f} \frac{\tau_T^3}{V_T} \psi_1(\sigma)\psi_2(\sigma) \, \mathrm{d}\sigma, \quad I_{23} \triangleq \int_t^{t_f} \frac{\tau_T}{V_T} \psi_2(\sigma)\psi_3(\sigma) \, \mathrm{d}\sigma$$

$$I_2 \triangleq \int_t^{t_f} \frac{\tau_T^2}{V_T^2} \psi_2(\sigma)^2 \, \mathrm{d}\sigma, \qquad I_3 \triangleq \int_t^{t_f} \psi_3(\sigma)^2 \, \mathrm{d}\sigma \tag{33}$$

If the tanker has perfect autopilot dynamics, that is $\tau_T \to 0$, the gains degenerate to those of the intercept angle guidance law for ideal dynamics presented in [10] $N_1(c_1, c_2 \to \infty, c_3 \to 0, \tau_T \to 0) = 6$, $N_2(c_1, c_2 \to \infty, c_3 \to 0, \tau_T \to 0) = 2$. If we choose $c_1 \to \infty$ and $c_3$, $c_2 \to 0$, which dictate zero miss only, the guidance law further degenerates to the optimal guidance law [15] with the gains

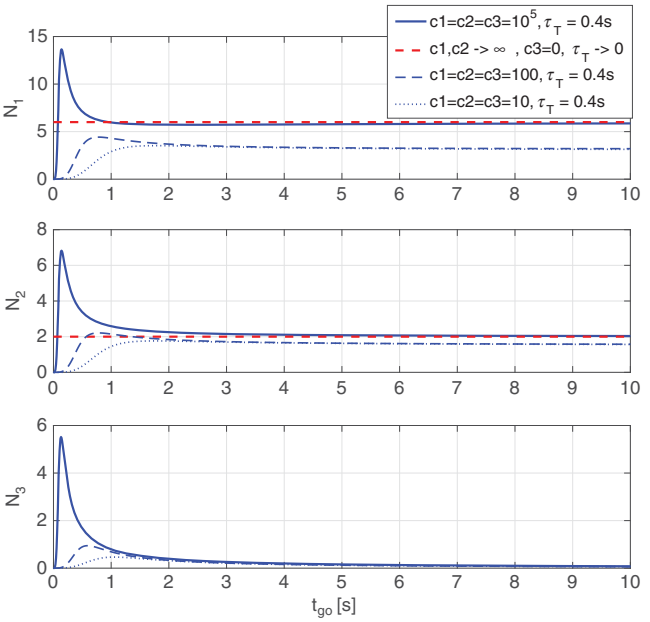


**Fig. 2 Navigation gains for SGC.**

$$N_1(c_1 \to \infty c_3, c_2 \to 0) = \frac{6\sigma^2(\sigma + e^{-\sigma} - 1)}{3 + 6\sigma - 6\sigma^2 + 2\sigma^3 - 12\sigma e^{-\sigma} - 3e^{-2\sigma}} \tag{34}$$

For perfect autopilot dynamics ($\tau_T \to 0$), the guidance gain Eq. (34) is reduced to the well-known optimal PN gain [15] $N_1(c_1 \to \infty c_3, c_2 \to 0, \tau_T \to 0) = 3$. The closed-form solution for the most-general limiting case where $c_1 \to \infty$, $c_2 \to \infty$, and $c_3 \to \infty$ is too cumbersome to be given here.

Figure 2 presents the numerically computed navigation gains as functions of $t_{\text{go}}$ for various values of the weight coefficients $c_1, c_2, c_3$ and for autopilot lag $\tau_T = 0.4$ s. For high weight coefficients, the produced gains increase sharply as $t_{\text{go}} \to 0$, near rendezvous to compensate the effect of the autopilot lag. However, because nonlinear effects of the aircraft dynamics at small $t_{\text{go}}$ can generate large guidance errors, sharp increase of the gains may result in instability. For large values of $t_{\text{go}}$, the guidance gains are constant and equal to those with no autopilot lag. This is due to the observation that mathematically $\tau_T \to 0$ is equivalent to $t_{\text{go}} \to \infty$, suggesting that, for large values of $t_{\text{go}}$, the effect of the autopilot lag is negligible. Also, it can be seen in the lowest plot that the additional penalty on the terminal acceleration has an effect for small values of $t_{\text{go}}$, whereas for large $t_{\text{go}}$, the guidance law is indifferent to this penalty, holding the value of $N_3$ practically at zero regardless of the value chosen for $c_3$.

## IV. Performance Evaluation

The guidance performance is evaluated using a high-fidelity simulation model available from previous studies on aerial refueling, implemented in Matlab Simulink. It consists of detailed nonlinear aircraft simulation models of four-engine civil transport aircraft, including engine and actuator dynamics and nonlinear aerodynamic models, based on exhaustive lookup tables that are scheduled over angle of attack, sideslip, and Mach number, just to mention the most important dependencies [16]. The simulation environment also includes a model for the wake interaction between the aircraft. Many available studies on wake interaction focus on the effect of larger leading on smaller trailing aircraft. To obtain reasonable numbers for the interaction between two large aircraft, estimation by the vortex lattice method and an extended lifting-line theory by Philips and Snyder [17] were used, where the latter constitutes an adaption of the classical lifting-line theory applying a three-dimensional vortex lifting law instead of the two-dimensional Kutta–Joukowski law usually used in classical theory. This allowed for estimation of force and moment increments due to wake interaction as a function of

relative position between the aircraft and angle of attack of the leading aircraft. The interaction proved to be qualitatively correct and quantitatively reasonable compared to typical computational-fluid-dynamics analysis and results of previous modeling and flight-test efforts [18,19], especially for close formation flight, where wake dissipation has only a low effect.

The analysis is based on a single scenario with the receiver aircraft flying at an altitude of 7620 m and 242 m/s airspeed. The tanker is initially flying at 235 m/s and located with the initial offset of $\boldsymbol{r}(t=0) = [250 \quad -100 \quad 200\ \text{m}]$ relative to the receiver and subjected to constant longitudinal acceleration to ensure smooth approach (for a duration of approximately 100 s) in the forward direction. The nominal value is used for the tanker speed $V_T = 240$ m/s for the gain calculation. For both architectures, the guidance gains become high at the last seconds of the approach. The high gains cause increased control commands (due to increased state errors resulting from combination of the wake and atmospheric disturbances), which hit the saturation limits in the nonlinear model. This effect is not considered in the model used for the guidance law development. The preceding problem is addressed by planning the guidance for longer time than expected for the approach. This results in termination of the guidance slightly earlier than planned and, in turn, small relative position errors. However, because the requirement of the approach maneuver is to position the tanker in the envelope reachable by the boom, those position errors are acceptable.

First, single-run performance will be illustrated both for SGC and IGC guidance architectures for various flight conditions. Next, performance criteria will be defined to evaluate and compare the guidance laws for various weight selections. Figure 3 presents sample run simulation results with SGC guidance architecture for two cases: nonturbulent environment and with light turbulence, both with the aerodynamic wake interaction effect. Figure 4 presents the simulation results for the same conditions with the IGC architecture. It can be seen that both architectures were able to steer the tanker toward rendezvous as required by the guidance objectives. For perfect atmospheric conditions, both guidance laws are able to reduce

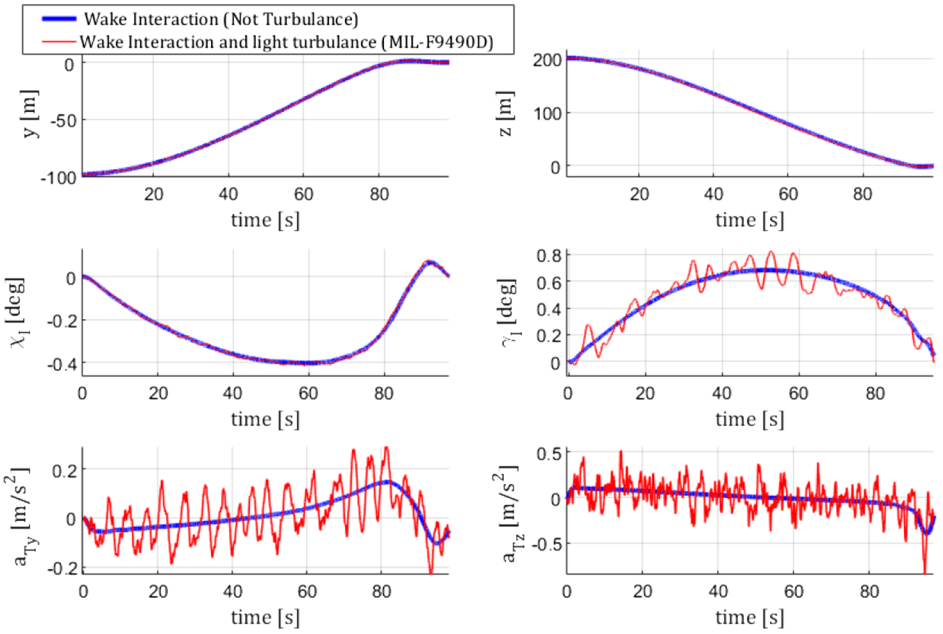


**Fig. 3 Sample run simulation results for SGC design with aerodynamic wake interaction and light turbulence.**

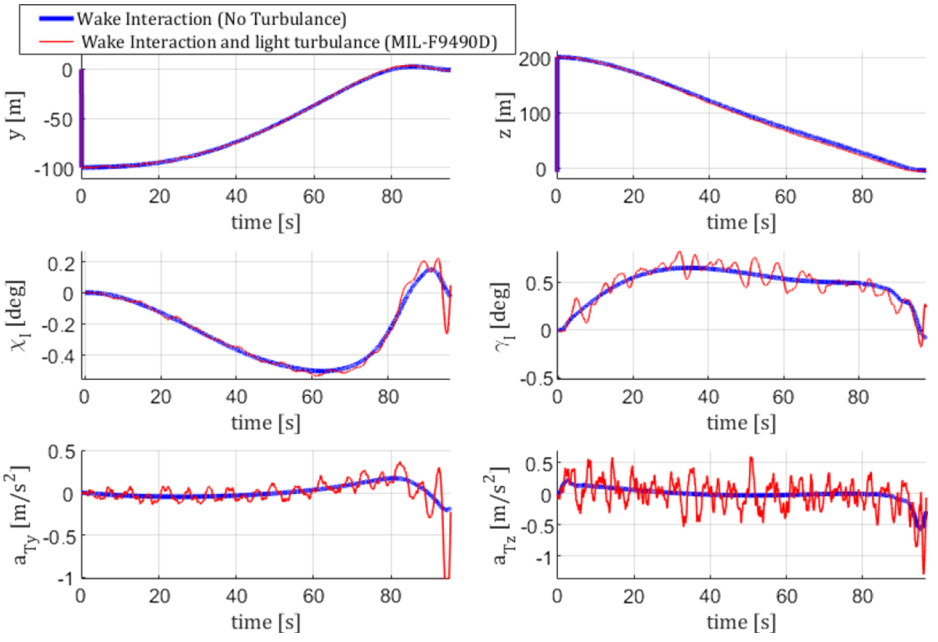


**Fig. 4 Sample run simulation results for IGC design with aerodynamic wake interaction and light turbulence.**

position, angle, and acceleration errors practically to zero. The effect of the tanker wake is evident from the time histories of the path angle and acceleration overshoots in the horizontal channel roughly for the last 8 s of the approach.

### A. Performance Comparison

To compare the performance of the SGC and IGC solutions, it is necessary to select a relevant performance criterion. One natural choice for a performance criterion would be the control effort used in the guidance law design. The control input in the SGC design (acceleration commands) is different from the control input used in IGC design (control surface deflection). Because, in the SGC loop, the control surface deflections are a function of the commanded acceleration, their time history can be used as a basis for the performance criterion. However, it turns out that the control surface deflections are generally very small for both solutions, and so they are poor indicators of the performance of the system. For nonideal environmental conditions, the performance of the two guidance laws is better evaluated and compared on the basis of the variation in the control surface deflections instead of the actual deflections. The performance criterion is selected as $\int \dot{\delta}_e^2 \, dt$ and $\int \dot{\delta}_a^2 \, dt$. The ability of the guidance law to shape the trajectory can be characterized by the integral of the position error trajectories squared. The trajectory shaping criterion is selected as $\int z^2 \, dt$ and $\int y^2 \, dt$.

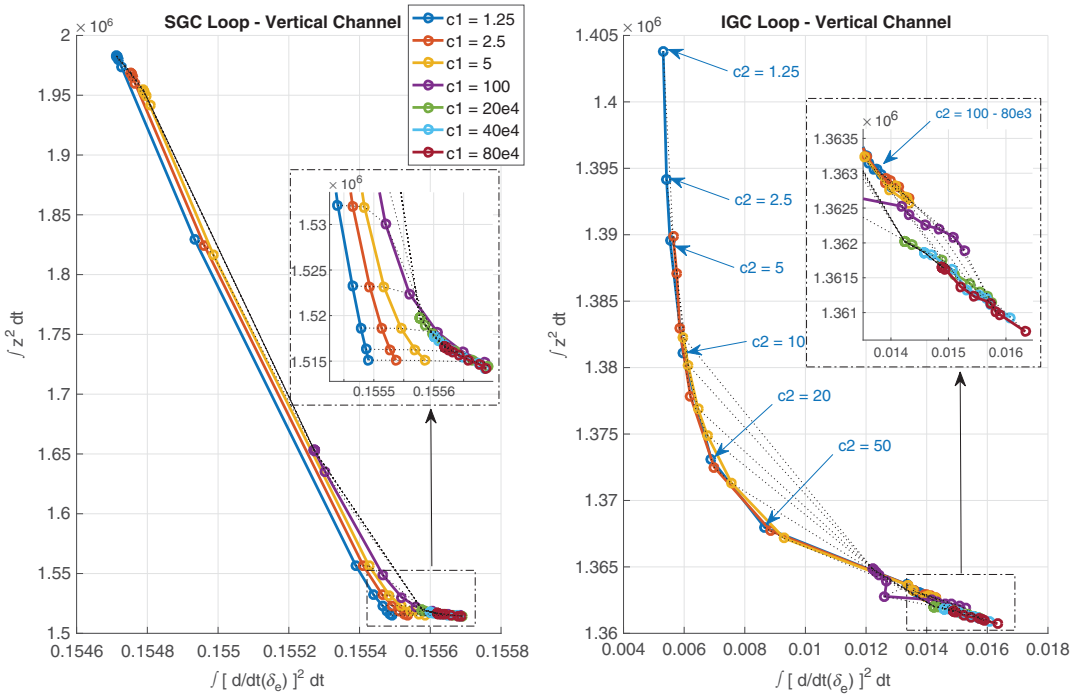


**Fig. 5 Simulation performance results for vertical channel, SGC vs IGC comparison (with aerodynamic interactions and turbulence).**

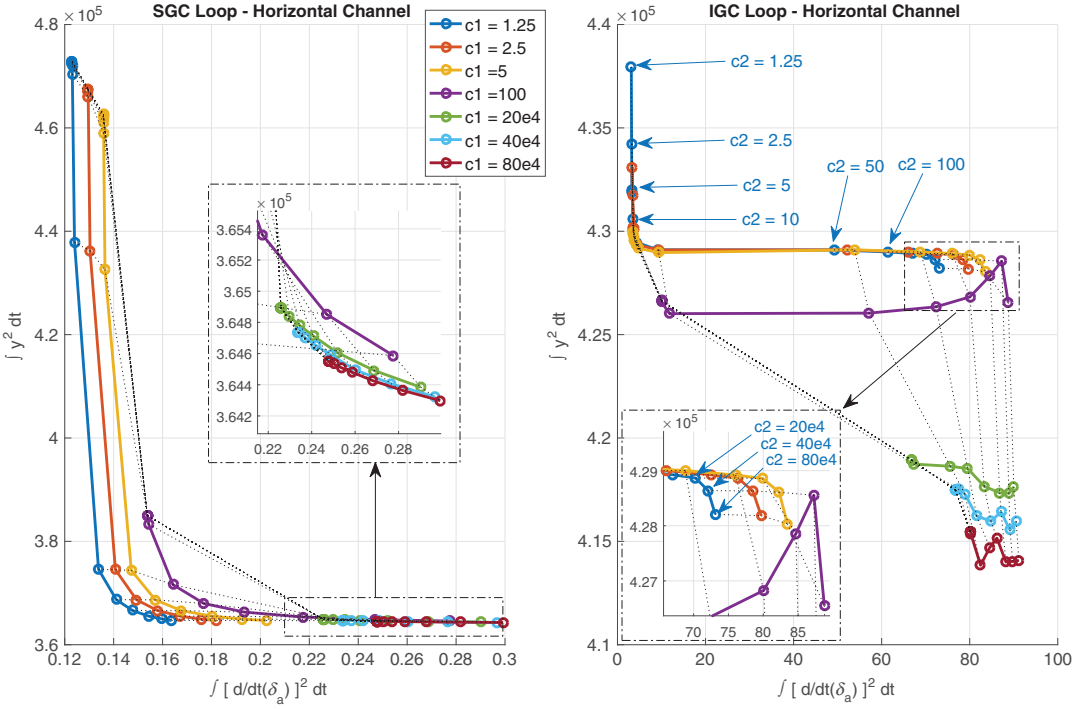


**Fig. 6 Simulation performance results for horizontal channel, SGC vs IGC comparison (with aerodynamic interactions and turbulence).**

Figures 5 and 6 present the results for the vertical and horizontal channels, respectively, from multiple simulation runs. Each circle represents a single simulation run with navigation gains calculated based on a different weight coefficients selection and plotted as function of the performance criterion defined previously. Better performance is claimed for circles that are located closer to the origin of the plot, indicating a selection of weight coefficients that result in good guidance performance in the sense of the ability of the guidance law to shape the trajectory with relatively small control variation. For example, as can be seen in Fig. 6, increasing $c_2$ weight coefficient above approximately 10 (for IGC in the right plot) and above approximately 50 (for SGC in the left plot) has negligible effect on the shaping of the trajectory while the control variation is increased. By comparing the results presented in Figs. 5 and 6, better performance of the IGC loop can be claimed in the vertical channel. This is caused by two factors. First, the noisy acceleration feedback in the vertical channel autopilot causes the SGC loop to steer the tanker much more aggressively, attempting to mitigate turbulence induced accelerations, whereas IGC behaves more smoothly to the induced accelerations. Second, the effect of the nonminimum phase response of the separate inner-loop autopilot to acceleration commands (which was explicitly accounted in IGC gain calculation) becomes dominant near the very end. Because acceleration command in one direction causes initially a relatively high acceleration in the opposite direction, and because it is not expected by the separated guidance algorithm, large control variations occur. The preceding suggests that, by using the IGC loop for the vertical channel and SGC loop for the horizontal channel, one may enhance overall performance in terms of control variation.

## V. Conclusions

This paper considers the problem of designing the approach phase for an automatic aerial refueling system in which the receiver is entirely passive, flying a straight and level trajectory, and the maneuver is executed solely by the tanker that is required to position itself in front of the receiver, before the deployment of the docking equipment. The problem is treated using methods previously developed for optimal guidance theory. To improve the performance of the system, taking into account the specific requirements posed by the aerial refueling operation, the usual constraints on the terminal relative position and relative approach angle are supplemented with a condition on the terminal acceleration. Two different methodologies are adopted for guidance algorithm design: a separate guidance loop design, which is based on a separate autopilot loop for tracking the vertical and lateral acceleration commands, and an integrated full-state single-loop guidance–autopilot design, which provides directly the control surface deflection commands for the tanker aircraft. The guidance and control method is capable of steering the tanker aircraft smoothly to achieve the required terminal configuration for the two aircraft under nonperfect atmospheric conditions. It is, however, not able to guarantee zero errors for the rendezvous problem because instability is exhibited toward the end of the maneuver. The instability arises due to nonlinear effects that were not taken into account in the model used in the development of the guidance laws. This instability can be alleviated by a correct selection of weight coefficients in the design process. Also, by planning the guidance for a longer time than expected for the approach phase, the instability can be reduced, without compromising the objective of the approach phase. A more detailed dynamic model, which elaborates the aerodynamic interaction of the aircraft in close proximity and the effect of velocity variation, may be used in the design process to enhance the guidance performance. The integrated guidance–autopilot loop showed slightly better performance in the vertical channel, and the separated guidance law exhibited better performance in the horizontal channel. Therefore, the overall guidance and control performance in terms of trajectory shaping and control effort variability can be improved by implementing a mixed SGC-IGC architecture.

## Appendix: Linear State-Space Tanker Models

The following state-space model matrices were obtained for nominal altitude of 7620 m, nominal speed of 240 m/s, and trim angle of attack of 2 deg:

$$\boldsymbol{A}_{T_z} = \begin{bmatrix} -0.488 & 0 & 0.9893 & 0.02 \\ 0 & 0 & 1 & 0 \\ -1.675 & 0 & -0.57 & 1.078 \\ 0 & 0 & 0 & -20 \end{bmatrix}$$

$$\boldsymbol{A}_{T_y} = \begin{bmatrix} -0.0915 & -0.995 & 0.042 & 0.034 & 0 \\ 1.264 & -0.222 & 0 & -0.033 & 0.025 \\ 0 & 0 & 0 & 1 & 0 \\ -4.316 & 0.466 & 0 & -0.9836 & 0.3961 \\ 0 & 0 & 0 & 0 & -20 \end{bmatrix}$$

$$\boldsymbol{B}_{T_z} = [0 \quad 0 \quad 0 \quad 20]^T, \qquad \boldsymbol{B}_{T_y} = [0 \quad 0 \quad 0 \quad 0 \quad 20]^T$$

## Acknowledgments

This research was supported by a grant from the German–Israeli foundation for scientific research and development.

## References

[1] McRoberts, R., Early, J. M., Morscheck, F., Price, M., and Korn, B., "Tanker Mission Implication on a Civil Aerial Refuelling Transport System's Benefit Evaluation," *Journal of Aircraft*, Vol. 52, No. 1, 2015, pp. 320–328.

[2] Nangia, R., and Martensson, T., "Towards Design of Efficient Concepts for Civil Air to Air Refuelling (AAR)," *Proceedings of the RAeS Conference on Advanced Aero Concepts, Design and Operations*, Bristol, England, U.K., 2014, pp. 22–24.

[3] Timmermans, H., and LaRocca, G., "Conceptual Design of a Flying Boom for Air-to-Air Refueling of Passenger Aircraft," *AIP Conference Proceedings*, Vol. 1618, No. 1, 2014, pp. 398–401.

[4] Ochi, Y., and Kominami, T., "Flight Control for Automatic Aerial Refueling via PNG and LOS Angle Control," *AIAA Guidance, Navigation and Control Conference and Exhibit*, AIAA Paper 2005-6268, Aug. 2005.

[5] Ratnoo, A., "Variable Deviated Pursuit for Rendezvous Guidance," *Journal of Guidance, Control, and Dynamics*, Vol. 38, No. 4, 2015, pp. 787–792. doi:10.2514/1.G000573

[6] Wang, J., Patel, V. V., Cao, C., Hovakimyan, N., and Lavretsky, E., "Novel L1 Adaptive Control Methodology for Aerial Refueling with Guaranteed Transient Performance," *Journal of Guidance, Control, and Dynamics*, Vol. 31, No. 1, 2008, pp. 182–193. doi:10.2514/1.31199

[7] Doebbler, J., Spaeth, T., Valasek, J., Monda, M. J., and Schaub, H., "Boom and Receptacle Autonomous Air Refueling Using Visual Snake Optical Sensor," *Journal of Guidance, Control, and Dynamics*, Vol. 30, No. 6, 2007, pp. 1753–1769. doi:10.2514/1.28305

[8] Fravolini, M. L., Ficola, A., Campa, G., Napolitano, M. R., and Seanor, B., "Modeling and Control Issues for Autonomous Aerial Refueling for UAVs Using a Probe–Drogue Refueling System," *Aerospace Science and Technology*, Vol. 8, No. 7, 2004, pp. 611–618. doi:10.1016/j.ast.2004.06.006

[9] Tandale, M. D., Bowers, R., and Valasek, J., "Trajectory Tracking Controller for Vision-Based Probe and Drogue Autonomous Aerial Refueling," *Journal of Guidance, Control, and Dynamics*, Vol. 29, No. 4, 2006, pp. 846–857. doi:10.2514/1.19694

[10] Shaferman, V., and Shima, T., "Linear Quadratic Guidance Laws for Imposing a Terminal Intercept Angle," *Journal of Guidance, Control, and Dynamics*, Vol. 31, No. 5, 2008, pp. 1400–1412. doi:10.2514/1.32836

[11] Ryoo, C. K., Cho, H., and Tahk, M. J., "Optimal Guidance Laws with Terminal Impact Angle Constraint," *Journal of Guidance, Control, and Dynamics*, Vol. 28, No. 4, 2005, pp. 724–732. doi:10.2514/1.8392

[12] Ratnoo, A., Hayoun, S. Y., Granot, A., and Shima, T., "Path Following Using Trajectory Shaping Guidance," *Journal of Guidance, Control, and Dynamics*, Vol. 38, No. 1, 2015, pp. 106–116. doi:10.2514/1.G000300

[13] Blakelock, J. H., *Automatic Control of Aircraft and Missiles*, Wiley, Hoboken, NJ, 1991.

[14] Palumbo, N. F., Reardon, B. E., and Blauwkamp, R. A., "Integrated Guidance and Control for Homing Missiles," *Johns Hopkins APL Technical Digest*, Vol. 25, No. 2, 2004, pp. 121–139.

[15] Palumbo, N. F., Blauwkamp, R. A., and Lloyd, J. M., "Modern Homing Missile Guidance Theory and Techniques," *Johns Hopkins APL Technical Digest*, Vol. 29, No. 1, 2010, pp. 42–59.

[16] Hanke, C. R., and Nordwall, D. R., "The Simulation of a Jumbo Jet Transport Aircraft. Volume 2, : Modeling Data," NASA Technical Rept. NASA-CR-114494, Boeing Co., Wichita, KS, 1970.

[17] Phillips, W., and Snyder, D., "Modern Adaptation of Prandtl's Classic Lifting-Line Theory," *Journal of Aircraft*, Vol. 37, No. 4, 2000, pp. 662–670. doi:10.2514/2.2649

[18] Dogan, A., Venkataramanan, S., and Blake, W., "Modeling of Aerodynamic Coupling Between Aircraft in Close Proximity," *Journal of Aircraft*, Vol. 42, No. 4, 2005, pp. 941–955. doi:10.2514/1.7579

[19] Dogan, A., Lewis, T. A., and Blake, W., "Flight Data Analysis and Simulation of Wind Effects During Aerial Refueling," *Journal of Aircraft*, Vol. 45, No. 6, 2008, pp. 2036–2048. doi:10.2514/1.36797